Physics Letters B 759 (2016) 69–74

Contents lists available at ScienceDirect

Physics Letters B

www.elsevier.com/locate/physletb

Limits on dark matter annihilation in the sun using the ANTARES neutrino telescope

S. Adrián-Martínez [a], A. Albert [b], M. André [c], G. Anton [d], M. Ardid [a], J.-J. Aubert [e], T. Avgitas [f], B. Baret [f], J. Barrios-Martí [g], S. Basa [h], V. Bertin [e], S. Biagi [i], R. Bormuth [j,k], M.C. Bouwhuis [j], R. Bruijn [j,l], J. Brunner [e], J. Busto [e], A. Capone [m,n], L. Caramete [o], J. Carr [e], S. Celli [m,n], T. Chiarusi [p], M. Circella [q], A. Coleiro [f], R. Coniglione [i], H. Costantini [e], P. Coyle [e], A. Creusot [f], A. Deschamps [r], G. De Bonis [m,n], C. Distefano [i], C. Donzaud [f,s], D. Dornic [e], D. Drouhin [b], T. Eberl [d], I. El Bojaddaini [t], D. Elsässer [u], A. Enzenhöfer [e], K. Fehn [d], I. Felis [a], L.A. Fusco [p,v], S. Galatà [f], P. Gay [w,2], S. Geißelsöder [d], K. Geyer [d], V. Giordano [x], A. Gleixner [d], H. Glotin [y,z,aa,1], R. Gracia-Ruiz [f], K. Graf [d], S. Hallmann [d], H. van Haren [ab], A.J. Heijboer [j], Y. Hello [r], J.J. Hernández-Rey [g], J. Hößl [d], J. Hofestädt [d], C. Hugon [ac,ad], G. Illuminati [m,n,g], C.W. James [d], M. de Jong [j,k], M. Jongen [j], M. Kadler [u], O. Kalekin [d], U. Katz [d], D. Kießling [d], A. Kouchner [f,1], M. Kreter [u], I. Kreykenbohm [ae], V. Kulikovskiy [i,af], C. Lachaud [f], R. Lahmann [d], D. Lefèvre [ag,ah], E. Leonora [x,ai], S. Loucatos [aj,2], M. Marcelin [h], A. Margiotta [p,v], A. Marinelli [ak,al], J.A. Martínez-Mora [a], A. Mathieu [e], K. Melis [j,l], T. Michael [j], P. Migliozzi [am], A. Moussa [t], C. Mueller [u], E. Nezri [h], G.E. Păvălaş [o], C. Pellegrino [p,v], C. Perrina [m,n], P. Piattelli [i], V. Popa [o], T. Pradier [an,ao], C. Racca [b], G. Riccobene [i], K. Roensch [d], M. Saldaña [a], D.F.E. Samtleben [j,k], A. Sánchez-Losa [g,q], M. Sanguineti [ac,ad], P. Sapienza [i], J. Schnabel [d], F. Schüssler [aj], T. Seitz [d], C. Sieger [d], M. Spurio [p,v], Th. Stolarczyk [aj], M. Taiuti [ac,ad], C. Tönnis [g,*], A. Trovato [i], M. Tselengidou [d], D. Turpin [e], B. Vallage [aj,2], C. Vallée [e], V. Van Elewyck [f], D. Vivolo [am,ap], S. Wagner [d], J. Wilms [ae], J.D. Zornoza [g], J. Zúñiga [g]

[a] Institut d'Investigació per a la Gestió Integrada de les Zones Costaneres (IGIC) – Universitat Politècnica de València, C/ Paranimf 1, 46730 Gandia, Spain
[b] GRPHE – Université de Haute Alsace – Institut universitaire de technologie de Colmar, 34 rue du Grillenbreit BP 50568 – 68008 Colmar, France
[c] Technical University of Catalonia, Laboratory of Applied Bioacoustics, Rambla Exposició, 08800 Vilanova i la Geltrú, Barcelona, Spain
[d] Friedrich–Alexander-Universität Erlangen–Nürnberg, Erlangen Centre for Astroparticle Physics, Erwin-Rommel-Str. 1, 91058 Erlangen, Germany
[e] Aix-Marseille Université, CNRS/IN2P3, CPPM UMR 7346, 13288 Marseille, France
[f] APC, Université Paris Diderot, CNRS/IN2P3, CEA/IRFU, Observatoire de Paris, Sorbonne Paris Cité, 75205 Paris, France
[g] IFIC – Instituto de Física Corpuscular, Edificios Investigación de Paterna, CSIC – Universitat de València, Apdo. de Correos 22085, 46071 Valencia, Spain
[h] LAM – Laboratoire d'Astrophysique de Marseille, Pôle de l'Étoile Site de Château-Gombert, rue Frédéric Joliot-Curie 38, 13388 Marseille Cedex 13, France
[i] INFN – Laboratori Nazionali del Sud (LNS), Via S. Sofia 62, 95123 Catania, Italy
[j] Nikhef, Science Park, Amsterdam, The Netherlands
[k] Huygens–Kamerlingh Onnes Laboratorium, Universiteit Leiden, The Netherlands
[l] Universiteit van Amsterdam, Instituut voor Hoge-Energie Fysica, Science Park 105, 1098 XG Amsterdam, The Netherlands
[m] INFN – Sezione di Roma, P. le Aldo Moro 2, 00185 Roma, Italy
[n] Dipartimento di Fisica dell'Università La Sapienza, P. le Aldo Moro 2, 00185 Roma, Italy
[o] Institute for Space Science, RO-077125 Bucharest, Măgurele, Romania
[p] INFN – Sezione di Bologna, Viale Berti-Pichat 6/2, 40127 Bologna, Italy
[q] INFN – Sezione di Bari, Via E. Orabona 4, 70126 Bari, Italy
[r] Géoazur, UCA, CNRS, IRD, Observatoire de la Côte d'Azur, Sophia Antipolis, France
[s] Univ. Paris-Sud, 91405 Orsay Cedex, France
[t] University Mohammed I, Laboratory of Physics of Matter and Radiations, B.P. 717, Oujda 6000, Morocco
[u] Institut für Theoretische Physik und Astrophysik, Universität Würzburg, Emil-Fischer Str. 31, 97074 Würzburg, Germany
[v] Dipartimento di Fisica e Astronomia dell'Università, Viale Berti Pichat 6/2, 40127 Bologna, Italy
[w] Laboratoire de Physique Corpusculaire, Clermont Univertsité, Université Blaise Pascal, CNRS/IN2P3, BP 10448, F-63000 Clermont-Ferrand, France
[x] INFN – Sezione di Catania, Viale Andrea Doria 6, 95125 Catania, Italy
[y] LSIS, Aix Marseille Université, CNRS, ENSAM, LSIS, UMR 7296, 13397 Marseille, France
[z] Université de Toulon, CNRS, LSIS, UMR 7296, 83957 La Garde, France

http://dx.doi.org/10.1016/j.physletb.2016.05.019

[aa] Institut Universitaire de France, 75005 Paris, France
[ab] Royal Netherlands Institute for Sea Research (NIOZ), Landsdiep 4, 1797 SZ 't Horntje (Texel), The Netherlands
[ac] INFN – Sezione di Genova, Via Dodecaneso 33, 16146 Genova, Italy
[ad] Dipartimento di Fisica dell'Università, Via Dodecaneso 33, 16146 Genova, Italy
[ae] Dr. Remeis-Sternwarte and ECAP, Universität Erlangen–Nürnberg, Sternwartstr. 7, 96049 Bamberg, Germany
[af] Moscow State University, Skobeltsyn Institute of Nuclear Physics, Leninskie Gory, 119991 Moscow, Russia
[ag] Mediterranean Institute of Oceanography (MIO), Aix-Marseille University, 13288, Marseille, Cedex 9, France
[ah] Université du Sud Toulon-Var, CNRS–INSU/IRD UM 110, 83957, La Garde Cedex, France
[ai] Dipartimento di Fisica ed Astronomia dell'Università, Viale Andrea Doria 6, 95125 Catania, Italy
[aj] Direction des Sciences de la Matière – Institut de recherche sur les lois fondamentales de l'Univers – Service de Physique des Particules, CEA Saclay, 91191 Gif-sur-Yvette Cedex, France
[ak] INFN – Sezione di Pisa, Largo B. Pontecorvo 3, 56127 Pisa, Italy
[al] Dipartimento di Fisica dell'Università, Largo B. Pontecorvo 3, 56127 Pisa, Italy
[am] INFN – Sezione di Napoli, Via Cintia, 80126 Napoli, Italy
[an] Université de Strasbourg, IPHC, 23 rue du Loess, 67037 Strasbourg, France
[ao] CNRS, UMR7178, 67037 Strasbourg, France
[ap] Dipartimento di Fisica dell'Università Federico II di Napoli, Via Cintia 80126, Napoli, Italy

ARTICLE INFO

Article history:
Received 7 March 2016
Received in revised form 27 April 2016
Accepted 6 May 2016
Available online 10 May 2016
Editor: S. Dodelson

Keywords:
Dark matter
WIMP
Neutralino
Indirect detection
Neutrino telescope
Sun

ABSTRACT

A search for muon neutrinos originating from dark matter annihilations in the Sun is performed using the data recorded by the ANTARES neutrino telescope from 2007 to 2012. In order to obtain the best possible sensitivities to dark matter signals, an optimisation of the event selection criteria is performed taking into account the background of atmospheric muons, atmospheric neutrinos and the energy spectra of the expected neutrino signals. No significant excess over the background is observed and 90% C.L. upper limits on the neutrino flux, the spin-dependent and spin-independent WIMP-nucleon cross-sections are derived for WIMP masses ranging from 50 GeV to 5 TeV for the annihilation channels WIMP + WIMP $\rightarrow b\bar{b}$, W^+W^- and $\tau^+\tau^-$.

1. Introduction

A number of independent observations in cosmology and astrophysics point to the existence of large amounts of non-baryonic matter in the Universe [1,2]. These observations indicate that there is approximately five times more of this dark matter than of ordinary baryonic matter.

A well-motivated hypothesis is that dark matter is composed of weakly interacting massive particles (WIMPs) that form halos in which galaxies are embedded. There are different candidates for these WIMPs, amongst which, those provided by supersymmetric models are currently the focus of the attention of a large variety of searches. In the case of the minimal supersymmetric extension of the Standard Model (MSSM), the lightest new particle is stable due to the conservation of a quantum number, the R-parity, that prevents its decay to ordinary particles [3]. If this lightest supersymmetric particle is also electromagnetically neutral, it is a natural WIMP candidate for dark matter. This lightest particle can annihilate into pairs of standard model particles. Neutrinos, in particular, are the final product of a large variety of decay processes, being therefore a good candidate for an indirect search for dark matter. WIMPs tend to accumulate in celestial objects due to scattering with ordinary matter and the gravitation pull of these objects. This is why indirect searches for dark matter concentrate on massive astrophysical bodies such as the Earth, the centre of our Galaxy, galaxy clusters or, as in this case, the Sun.

In this letter, an indirect search for neutrinos coming from WIMP annihilations in the Sun is presented, using data recorded by the ANTARES neutrino telescope from 2007 to 2012. Different quality cuts on the data have been used to reduce the atmospheric background and optimise the sensitivity of the analysis. Sensitivities to the signal neutrino flux, Φ_ν, and the spin-dependent and spin-independent WIMP-nucleon cross-sections, $\sigma^{\rm p}_{\rm SD}$ and $\sigma_{\rm SI}$, are derived using three different annihilation channels.

2. The ANTARES neutrino telescope

The ANTARES detector [4,5] is an undersea neutrino telescope anchored 2475 m below the surface of the Mediterranean Sea and 40 km offshore from Toulon (France) at 42°48′ N and 6°10′ E. ANTARES consists of 12 detection lines with 25 storeys per line and 3 optical modules with 10″ photomultipliers per storey. The detection lines are 450 m long and 60–75 m apart horizontally. Data taking started in 2007, when the first five lines of ANTARES were installed. The detector installation was completed in May 2008.

The main channel through which neutrinos are detected is via the muons produced from high-energy muon neutrinos interacting inside, or in the vicinity of, the detector. These muons move at relativistic velocities and induce the emission of Cherenkov light that is then detected by the optical modules. In this analysis, only muon neutrinos detected this way will be considered. In the following any mention of 'neutrinos' will refer to muon neutrinos and muon antineutrinos.

The flux of atmospheric muons from above the detector comprises the largest part of the background, with fluxes several orders of magnitude larger than any expected signal. In order to reduce the number of atmospheric muons, a cut on the elevation of reconstructed muon tracks is applied, ensuring that only events that have been reconstructed as upgoing are used. Since muons can-

* Corresponding author.
E-mail address: ctoennis@ific.uv.es (C. Tönnis).
[1] Institut Universitaire de France, 75005 Paris, France.
[2] Also at APC.

not cross the entire Earth, this cut rejects all atmospheric muons except for a small fraction of misreconstructed events. The atmospheric neutrinos represent the irreducible background for this search.

Atmospheric neutrinos from 10 GeV to 20 TeV are generated in the simulation using the standard ANTARES simulation chain [6–11].

The expected neutrino energy spectra from WIMP annihilations in the Sun are calculated with the WIMPSim simulation package [12]. The code takes into account the absorption of neutrinos in the solar plasma and the neutrino oscillation inside the Sun and on their way from the Sun to the detector. Neutrino spectra are calculated for 15 WIMP masses ranging from 50 GeV to 5 TeV and three annihilation channels assuming a branching ratio of 100%:

$$\mathrm{WIMP} + \mathrm{WIMP} \rightarrow b\bar{b}, \tau^+\tau^-, W^+W^-. \tag{1}$$

As shown in [13], the distribution of the number of muon neutrinos arriving at the Earth per pair of WIMPs self-annihilating in the Sun's core provides hard spectra for the $\tau^+\tau^-$ and W^+W^- and a soft spectrum for $b\bar{b}$. Limits calculated for dark matter candidate models will lie between these three channels, depending on their branching ratios. The energy spectrum of each channel (see Fig. 2 in [13]) is used to calculate the acceptance for the particular annihilation channel in Equation (1). The acceptance is the neutrino effective area convoluted with the energy spectrum corresponding to a given WIMP mass (see Section 3).

Two reconstruction algorithms are used in this paper. The first one is based on the minimisation of a χ^2-like quality parameter, Q, of the reconstruction which uses the difference between the expected and measured times of the detected photons, taking into account the effect of light absorption in the water [14]. The second algorithm consists of a multistep procedure to fit the direction of the muon track by maximising a likelihood ratio, Λ, which describes the quality of the reconstruction [15]. In addition to the Λ parameter, the uncertainty of the muon track angle, β, is used for the track selection. These two algorithms are respectively called here QFit and ΛFit. In order to reach the best efficiency of reconstruction in the entire neutrino energy range QFit is used for muon events reconstructed in a single detection line (single-line events), and ΛFit for muon events reconstructed on more than one detection line (multi-line events).

Extensive comparisons between data and simulations have been made elsewhere [16].

3. Analysis strategy

The search for WIMP annihilation in the Sun is performed based on a maximum-likelihood analysis method. The maximisation of this likelihood function, which is fed with the known information about the characteristics of the expected background and signal, provides an estimate of the amount of signal in the data. The extended likelihood function used for ΛFit is

$$\mathcal{L}(n_s) = e^{-(n_s+N_{\mathrm{bg}})} \prod_{i=1}^{N_{\mathrm{tot}}} \left(n_s S(\psi_i, N_{hit,i}, \beta_i) + N_{\mathrm{bg}} B(\psi_i, N_{hit,i}, \beta_i)\right), \tag{2}$$

where N_{bg} is the expected number of background events, N_{tot} is the total number of reconstructed events, n_s (the variable that changes during the maximisation process) is the number of signal events in the likelihood function, S and B are functions that calculate the likelihood of an event to be either signal or background, ψ_i is the angular distance of the i-th event to the Sun, $N_{hit,i}$ is the number of hits used in the reconstruction of the i-th event, which is used as an energy estimate and β_i is the value of the angular error estimate for the i-th event. S is calculated from the simulation and B is calculated from time-scrambled data.

For the QFit analysis the likelihood function looks different since for that analysis only single-line events have been used. For these events the azimuth angle can not be determined, so that the difference between the zenith angle of the events and the Sun has to be used instead of ψ:

$$\mathcal{L}(n_s) = e^{-(n_s+N_{\mathrm{bg}})} \prod_{i=1}^{N_{\mathrm{tot}}} \left(n_s \bar{S}(\theta_i, \bar{N}_{hit,i}, Q_i) + N_{\mathrm{bg}} \bar{B}(\theta_i, \bar{N}_{hit,i}, Q_i)\right), \tag{3}$$

where $\bar{N}_{hit,i}$ is the number of hits summed up per storey used for the reconstruction and θ_i is the difference in zenith angle between the i-th event and the Sun. $\bar{S}$ and $\bar{B}$ are analogous to S and B in the likelihood function used for the ΛFit data.

The angular resolution, which is used in S, is limited by the kinematic angle between neutrino and outgoing muon [16].

In this analysis a blinding protocol is applied for optimising the event selection. Blinding is achieved by using simulations to calculate the sensitivities, and time-scrambled data for calculating the background estimate.

In order to compute sensitivities and limits, 10^4 *pseudo-experiments* are performed for each combination of WIMP mass, annihilation channel and reconstruction strategy and for each considered value of n_s ($n_s \in \{0, 1, 2 \ldots 20\}$). In a pseudo-experiment, a random distribution of background events is simulated according to the features of the recorded data by randomising the right ascension of the events. Simulated signal events are introduced into these pseudo-experiments. These events are generated using the PSF and the signal characteristics for a given reference flux, which are also used in the likelihood function. For each pseudo-experiment, n_s is varied to maximise the likelihood function (when $n_s = n_{\max}$). The test statistic (TS) is then calculated as

$$\mathrm{TS} = \log_{10}\left(\frac{\mathcal{L}(n_{\max})}{\mathcal{L}(0)}\right). \tag{4}$$

Distributions of TS values are generated for different numbers of injected signal events. The overlap of TS distributions with inserted signal events and the TS distribution with only background is a measure of the likelihood to mistake pure background for an event distribution with a certain amount of signal in it. From this, the 90% C.L. sensitivities in terms of detected signal events, $\mu_{90\%}$, are obtained using the Neyman method for generating limits [17]. The so-defined $\mu_{90\%}$ quantity corresponds to the lowest number of signal events so that 90% of pseudo-experiments provide TS values above the median of the TS distribution of the pure background case.

Event selection consists of cuts on the quality parameters Λ and Q of the two reconstructions that are used in this analysis. These cuts are optimised with respect to the sensitivities (i.e. the model rejection factor). The optimum cuts for the relevant mass ranges are $\Lambda > -5.4$ and $\beta < 1^\circ$ for ΛFit and $Q < 0.8$ for the QFit analysis.

The sensitivities in terms of neutrino fluxes are calculated using the acceptance, defined as

$$\begin{aligned}\mathcal{A}^j(M_{\mathrm{WIMP}}) = &\int_{E_{th}}^{M_{\mathrm{WIMP}}} A^j_{\mathrm{eff}}(E_{\nu_\mu}) \left.\frac{d\Phi_{\nu_\mu}}{dE_{\nu_\mu}}\right|_{ch} dE_{\nu_\mu} \cdot T^j_{\mathrm{eff}} \\ &+ \int_{E_{th}}^{M_{\mathrm{WIMP}}} A^j_{\mathrm{eff}}(E_{\bar{\nu}_\mu}) \left.\frac{d\Phi_{\bar{\nu}_\mu}}{dE_{\bar{\nu}_\mu}}\right|_{ch} dE_{\bar{\nu}_\mu} \cdot T^j_{\mathrm{eff}},\end{aligned} \tag{5}$$

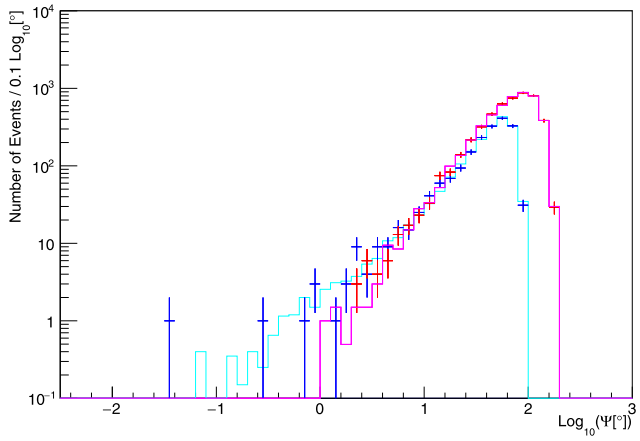

Fig. 1. Distribution of the angular distance between reconstructed the track direction of events and the Sun position for the ΛFit (red and pink) and QFit (blue and cyan) data samples (crosses) compared to the background estimates (histograms). For QFit the x-axis represents the logarithmic difference in zenith angle between event and Sun. (For interpretation of the references to colour in this figure legend, the reader is referred to the web version of this article.)

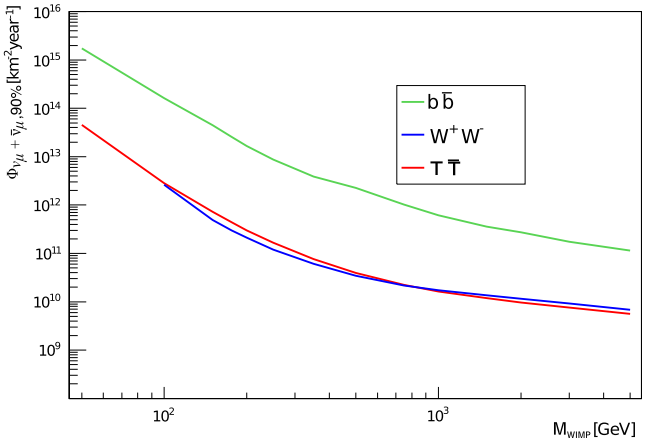

Fig. 2. Limits on a neutrino flux coming from the Sun as a function of the WIMP masses for the different channels considered.

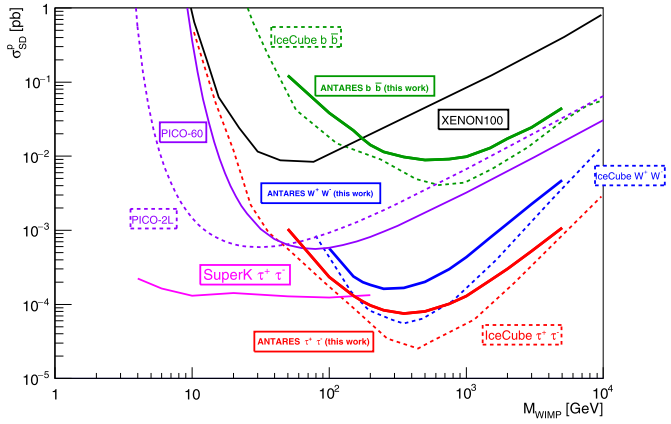

Fig. 3. Limits on the spin-dependent WIMP-nucleon scattering cross-section as a function of WIMP mass for the $b\bar{b}$, $\tau^+\tau^-$ and W^+W^- channels. Limits given by other experiments are also shown: IceCube [20], PICO-60 [21], PICO-2L [22], SuperK [23], XENON100 [24].

where $A^j_{\text{eff}}(E_{\nu_\mu})$ and $A^j_{\text{eff}}(E_{\bar{\nu}_\mu})$ are the effective areas for the j-th detector configuration period (see below) as a function of the muon neutrino energy, E_{ν_μ}, or muon antineutrino energy, $E_{\bar{\nu}_\mu}$, $\left.\frac{d\Phi_{\nu_\mu}}{dE_{\nu_\mu}}\right|_{ch}$ is the signal neutrino spectrum at the position of the detector for the annihilation channel ch (see Equation (1)), E_{th} is the energy threshold of the detector, M_{WIMP} is the WIMP mass and T^j_{eff} is the effective live time for the j-th detector configuration period. The effective area is defined as a 100% efficient equivalent area which would produce the same event rate as the detector. It is calculated from simulation. Throughout the lifetime of ANTARES the number of available detector lines has changed. The acceptance for the whole lifetime $\bar{\mathcal{A}}$ is calculated as the sum over the acceptances for all detector configuration periods.

The 90% C.L. sensitivities on the neutrino fluxes are then calculated as

$$\bar{\Phi}_{\nu_\mu+\bar{\nu}_\mu,90\%} = \frac{\bar{\mu}_{90\%}(M_{\text{WIMP}})}{\bar{\mathcal{A}}(M_{\text{WIMP}})}, \tag{6}$$

where $\bar{\mu}_{90\%}$ is the 90% C.L. sensitivity obtained from the likelihood function.

4. Results and discussion

In Fig. 1 it can be seen that there is no excess of events large enough to be identified as signal by the likelihood function. The median of the PSF used in the likelihood function is for most masses below 2 degrees. The observed TS is used to extract 90% C.L. upper limits from the absence of signal. However, since the observed value of the TS turns out to be smaller than the median of the TS distribution of pure background for all masses and channels, the sensitivity has been considered as the limit.

In Fig. 2 the limits on the neutrino flux from the Sun as a function of the WIMP mass are shown. In Fig. 2 the QFit and ΛFit results are combined. ΛFit gives the best flux limits in the W^+W^- decay channel at all WIMP masses, for $M_{\text{WIMP}} > 100$ GeV in the $\tau^+\tau^-$ channel and for $M_{\text{WIMP}} > 250$ GeV in the $b\bar{b}$ decay channel.

The limit on the total number of neutrinos from WIMP annihilations in the sun per unit of time C_n is calculated by

$$C_n = 4\pi d^2_{\text{Sun},rms}\Phi_{\nu_\mu+\bar{\nu}_\mu,90\%}, \tag{7}$$

where $\Phi_{\nu_\mu+\bar{\nu}_\mu,90\%}$ is the limit on the neutrino flux and $d^2_{\text{Sun},rms}$ is the mean squared distance from the detector to the Sun. From this, the annihilation rate is calculated by dividing C_n by the average number of neutrinos per annihilation, as obtained by WIMPSim. The sensitivities on the spin-dependent and spin-independent scattering cross-sections are calculated from this annihilation rate assuming an equilibrium between annihilation and capture via scattering [18]. This means that the capture rate is twice as high as the annihilation rate. For the calculation of the capture rate a Maxwellian velocity distribution of the WIMPs with a root mean square velocity of 270 m s^{-1} and a local dark matter density of 0.4 GeV cm^{-3} is assumed [19]. Therefore, once the average number of neutrinos per annihilation is known, the annihilation rate and consequently the capture rate and the scattering cross-sections can be calculated.

All results are shown in comparison to the results of other experiments in Figs. 3 and 4 and summarised for reference in Table 1. Recently an update on the spin-dependent cross-section limits from the IceCube collaboration has been released [20]. These new limits show an improvement of up to a factor of 4 with respect to the previous limits by using the energy information of the events in the likelihood function. In the analysis presented here the inclusion of further event parameters (e.g. N_{hit}, β and Q in Equations (2) and (3)) leads to an improvement of a factor of up to 1.7. At WIMP masses of up to a few 100 GeV, the consistent strengthening of the flux limit with increasing WIMP mass (see Fig. 2) determines the behaviour of the cross-section limits. Above

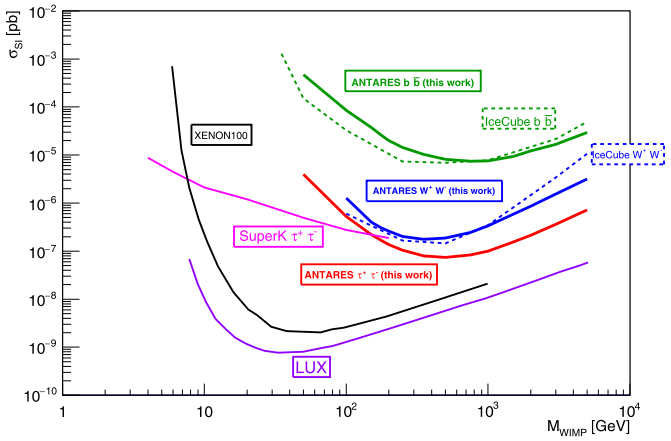

Fig. 4. Limits on the spin-independent WIMP-nucleon scattering cross-section as a function of WIMP mass for the different channels considered. Limits given by other experiments are also shown: IceCube [25], SuperK [23], LUX [26], XENON100 [27].

a WIMP mass of a few 100 GeV the factor of M_{WIMP}^{-2} in the conversion from neutrino flux to the scattering cross-sections dominates the behaviour of the cross-section limits and causes a rise with the WIMP mass. As a result, the cross-section limits show a minimum at a few 100 GeV.

The possible uncertainties on the background have been circumvented by using time-scrambled data for generating the background function B in the likelihood function. The largest systematic error is an uncertainty of 20% on the angular acceptance of the PMTs [28] and leads to a degradation of the detector efficiency (i.e. the acceptance) of 6% [13]. This effect has been taken into account for the limits presented here.

5. Conclusion

A new analysis searching for a signal of dark matter annihilations in the Sun has been conducted using the ANTARES data from 2007 to 2012. The unblinded data showed no significant excess above the background estimate and 90% confidence level exclusion limits have been calculated for the three annihilation channels WIMP + WIMP $\rightarrow b\bar{b}, W^+W^-, \tau^+\tau^-$ and WIMP masses ranging from 50 GeV to 5 TeV.

Acknowledgements

The authors acknowledge the financial support of the funding agencies: Centre National de la Recherche Scientifique (CNRS), Commissariat à l'Énergie Atomique et aux Énergies Alternatives (CEA), Commission Européenne (FEDER fund and Marie Curie Program), Institut Universitaire de France (IUF), IdEx program and UnivEarthS Labex program at Sorbonne Paris Cité (ANR-10-LABX-0023 and ANR-11-IDEX-0005-02), Région Île-de-France (DIM-ACAV), Région Alsace (contrat CPER), Région Provence-Alpes-Côte d'Azur, Département du Var and Ville de La Seyne-sur-Mer, France; Bundesministerium für Bildung und Forschung (BMBF), Germany; Istituto Nazionale di Fisica Nucleare (INFN), Italy; Stichting voor Fundamenteel Onderzoek der Materie (FOM), Nederlandse Organisatie voor Wetenschappelijk Onderzoek (NWO), the Netherlands; Council of the President of the Russian Federation for young scientists and leading scientific schools supporting grants, Russia; National Authority for Scientific Research (ANCS), Romania; Ministerio de Economía y Competitividad (MINECO), Severo Ochoa Centre of Excellence, MultiDark Consolider, Prometeo and Grisolía programs of Generalitat Valenciana, Spain; Agence de l'Oriental and CNRST, Morocco. We also acknowledge the technical support of IFREMER, AIM and Foselev Marine for the sea operation and the CC-IN2P3 for the computing facilities.

Table 1
Upper limits to neutrino flux, spin-dependent and spin-independent cross-section for different annihilation channels and WIMP masses. Limits for the W^+W^- channel cannot be produced for WIMP masses below the mass of the W boson.

M_{WIMP} [GeV]		Φ_ν [km^{-2} yr^{-1}]	σ^p_{SD} [pb]	σ_{SI} [pb]
50	$b\bar{b}$	$1.86 \cdot 10^{15}$	0.129	$4.98 \cdot 10^{-4}$
	$\tau\bar{\tau}$	$4.80 \cdot 10^{13}$	$1.10 \cdot 10^{-3}$	$4.23 \cdot 10^{-6}$
100	$b\bar{b}$	$1.73 \cdot 10^{14}$	$4.04 \cdot 10^{-2}$	$9.05 \cdot 10^{-5}$
	W^+W^-	$2.77 \cdot 10^{12}$	$6.01 \cdot 10^{-4}$	$1.35 \cdot 10^{-6}$
	$\tau\bar{\tau}$	$3.02 \cdot 10^{12}$	$2.48 \cdot 10^{-4}$	$5.55 \cdot 10^{-7}$
150	$b\bar{b}$	$4.78 \cdot 10^{13}$	$2.36 \cdot 10^{-2}$	$4.00 \cdot 10^{-5}$
	W^+W^-	$5.23 \cdot 10^{11}$	$2.52 \cdot 10^{-4}$	$4.26 \cdot 10^{-7}$
	$\tau\bar{\tau}$	$7.69 \cdot 10^{11}$	$1.39 \cdot 10^{-4}$	$2.35 \cdot 10^{-7}$
176	$b\bar{b}$	$2.70 \cdot 10^{13}$	$1.81 \cdot 10^{-2}$	$2.77 \cdot 10^{-5}$
	W^+W^-	$3.18 \cdot 10^{11}$	$2.12 \cdot 10^{-4}$	$3.24 \cdot 10^{-7}$
	$\tau\bar{\tau}$	$4.67 \cdot 10^{11}$	$1.15 \cdot 10^{-4}$	$1.77 \cdot 10^{-7}$
200	$b\bar{b}$	$1.76 \cdot 10^{13}$	$1.51 \cdot 10^{-2}$	$2.13 \cdot 10^{-5}$
	W^+W^-	$2.25 \cdot 10^{11}$	$1.95 \cdot 10^{-4}$	$2.71 \cdot 10^{-7}$
	$\tau\bar{\tau}$	$3.19 \cdot 10^{11}$	$1.10 \cdot 10^{-4}$	$1.43 \cdot 10^{-7}$
250	$b\bar{b}$	$8.75 \cdot 10^{12}$	$1.15 \cdot 10^{-2}$	$1.43 \cdot 10^{-5}$
	W^+W^-	$1.25 \cdot 10^{11}$	$1.72 \cdot 10^{-4}$	$2.15 \cdot 10^{-7}$
	$\tau\bar{\tau}$	$1.75 \cdot 10^{11}$	$8.82 \cdot 10^{-5}$	$1.10 \cdot 10^{-7}$
350	$b\bar{b}$	$4.11 \cdot 10^{12}$	$1.03 \cdot 10^{-2}$	$1.09 \cdot 10^{-5}$
	W^+W^-	$6.46 \cdot 10^{10}$	$1.77 \cdot 10^{-4}$	$1.88 \cdot 10^{-7}$
	$\tau\bar{\tau}$	$8.03 \cdot 10^{10}$	$7.95 \cdot 10^{-5}$	$8.44 \cdot 10^{-8}$
500	$b\bar{b}$	$2.37 \cdot 10^{12}$	$9.36 \cdot 10^{-3}$	$8.64 \cdot 10^{-6}$
	W^+W^-	$3.67 \cdot 10^{10}$	$2.13 \cdot 10^{-4}$	$1.98 \cdot 10^{-7}$
	$\tau\bar{\tau}$	$4.20 \cdot 10^{10}$	$8.48 \cdot 10^{-5}$	$7.82 \cdot 10^{-8}$
750	$b\bar{b}$	$1.08 \cdot 10^{12}$	$9.68 \cdot 10^{-3}$	$7.95 \cdot 10^{-6}$
	W^+W^-	$2.29 \cdot 10^{10}$	$3.16 \cdot 10^{-4}$	$2.59 \cdot 10^{-7}$
	$\tau\bar{\tau}$	$2.36 \cdot 10^{10}$	$1.07 \cdot 10^{-4}$	$8.82 \cdot 10^{-8}$
1000	$b\bar{b}$	$6.52 \cdot 10^{11}$	$1.04 \cdot 10^{-2}$	$8.03 \cdot 10^{-6}$
	W^+W^-	$1.83 \cdot 10^{10}$	$4.59 \cdot 10^{-4}$	$3.55 \cdot 10^{-7}$
	$\tau\bar{\tau}$	$1.72 \cdot 10^{10}$	$1.37 \cdot 10^{-4}$	$1.06 \cdot 10^{-7}$
1500	$b\bar{b}$	$3.79 \cdot 10^{11}$	$1.37 \cdot 10^{-2}$	$9.95 \cdot 10^{-6}$
	W^+W^-	$1.44 \cdot 10^{10}$	$8.47 \cdot 10^{-4}$	$6.15 \cdot 10^{-7}$
	$\tau\bar{\tau}$	$1.26 \cdot 10^{10}$	$2.24 \cdot 10^{-4}$	$1.63 \cdot 10^{-7}$
2000	$b\bar{b}$	$2.88 \cdot 10^{11}$	$1.82 \cdot 10^{-2}$	$1.28 \cdot 10^{-5}$
	W^+W^-	$1.21 \cdot 10^{10}$	$1.30 \cdot 10^{-3}$	$9.17 \cdot 10^{-7}$
	$\tau\bar{\tau}$	$1.03 \cdot 10^{10}$	$3.20 \cdot 10^{-4}$	$2.25 \cdot 10^{-7}$
3000	$b\bar{b}$	$1.82 \cdot 10^{11}$	$2.60 \cdot 10^{-2}$	$1.78 \cdot 10^{-5}$
	W^+W^-	$9.73 \cdot 10^{9}$	$2.44 \cdot 10^{-3}$	$1.63 \cdot 10^{-6}$
	$\tau\bar{\tau}$	$8.01 \cdot 10^{9}$	$5.57 \cdot 10^{-4}$	$3.81 \cdot 10^{-7}$
5000	$b\bar{b}$	$1.20 \cdot 10^{11}$	$4.71 \cdot 10^{-2}$	$3.15 \cdot 10^{-5}$
	W^+W^-	$7.25 \cdot 10^{9}$	$5.02 \cdot 10^{-3}$	$3.36 \cdot 10^{-6}$
	$\tau\bar{\tau}$	$5.02 \cdot 10^{9}$	$1.13 \cdot 10^{-3}$	$7.62 \cdot 10^{-7}$

References

[1] M. Klasen, M. Pohl, G. Sigl, Prog. Part. Nucl. Phys. 85 (2015).
[2] G. Bertone, D. Hooper, J. Silk, Phys. Rep. 405 (2005) 279.
[3] S. Martin, hep-ph/9709356v6, 2011.
[4] ANTARES Collaboration, M. Ageron, et al., Nucl. Instum. Methods Phys. Res. A 656 (2011) 11.
[5] ANTARES Collaboration, S. Adrian-Martinez, et al., J. Instrum. 7 (2012) T08002.
[6] J. Brunner, in: Proceedings of the VLVnT Workshop, Amsterdam, The Netherlands, 2003, p. 109.
[7] G. Carminati, M. Bazzotti, A. Margiotta, M. Spurio, Comput. Phys. Commun. 179 (2008) 915.
[8] A. Margiotta, Nucl. Instum. Methods A 725 (2012) 98.
[9] ANTARES Collaboration, J.A. Aguilar, et al., Astropart. Phys. 23 (2005) 131.

[10] ANTARES Collaboration, P. Amram, et al., Nucl. Instum. Methods Phys. Res. A 484 (2002) 369.
[11] ANTARES Collaboration, P. Amram, et al., Astropart. Phys. 19 (2003) 253.
[12] M. Blennow, J. Edsjo, T. Ohlsson, J. Cosmol. Astropart. Phys. 0801 (2008) 021.
[13] ANTARES Collaboration, S. Adrian-Martinez, et al., J. Cosmol. Astropart. Phys. 11 (2013).
[14] ANTARES Collaboration, J.A. Aguilar, et al., Astropart. Phys. 34 (2011) 652.
[15] ANTARES Collaboration, S. Adrian-Martinez, et al., Astrophys. J. 760 (2012).
[16] ANTARES Collaboration, S. Adrian-Martinez, et al., J. Cosmol. Astropart. Phys. 068 (2015).
[17] J. Neyman, Philos. Trans. R. Soc. Lond., Ser. A. 236 (1937) 250.
[18] W.H. Press, D.N. Spergel, Astrophys. J. 296 (1985) 679.
[19] G. Wikström, J. Edsjö, J. Cosmol. Astropart. Phys. 0904 (2009).
[20] IceCube Collaboration, M.G. Aartsen, et al., J. Cosmol. Astropart. Phys. 1604 (2016) 022.
[21] PICO Collaboration, C. Amole, et al., Phys. Rev. D 93 (2016) 052014.
[22] PICO Collaboration, C. Amole, et al., Phys. Rev. D 93 (2016) 061101.
[23] Super-Kamiokande Collaboration, K. Choi, et al., Phys. Rev. Lett. 114 (2015) 141301.
[24] XENON100 Collaboration, E. Aprile, et al., Phys. Rev. Lett. 111 (2013) 021301.
[25] IceCube Collaboration, M.G. Aartsen, et al., Phys. Rev. Lett. 110 (2013) 131302.
[26] LUX Collaboration, D.S. Akerib, et al., Phys. Rev. Lett. 112 (2014) 091303.
[27] XENON100 Collaboration, E. Aprile, et al., Phys. Rev. Lett. 109 (2012) 181301.
[28] ANTARES Collaboration, J.A. Aguilar, et al., Astropart. Phys. 34 (2011) 539.